Title

Associations between age and brain microstructure in older community-dwelling men and women: the Rancho Bernardo Study.

Authors

Hagler, Donald
Andrews, Murray
Lee, Roland
et al.

Publication Date

2020-11-01

DOI

10.1016/j.neurobiolaging.2020.07.007

Peer reviewed

HHS Public Access

Author manuscript

Neurobiol Aging. Author manuscript; available in PMC 2021 November 01.

Published in final edited form as:

Neurobiol Aging. 2020 November ; 95: 94–103. doi:10.1016/j.neurobiolaging.2020.07.007.

Associations between age and brain microstructure in older community-dwelling men and women: The Rancho Bernardo Study

Emilie T. Reas, PhD[a], **Donald J. Hagler Jr., PhD**[b], **Murray J. Andrews**[a], **Roland R. Lee**[b,c], **Anders M. Dale**[a,b], **Linda K. McEvoy, PhD**[b,d]

[a]Department of Neurosciences, University of California, San Diego

[b]Department of Radiology, University of California, San Diego

[c]Radiology Services, VA San Diego Healthcare System

[d]Department of Family Medicine and Public Health, University of California, San Diego

Abstract

Cytoarchitectural brain changes within gray matter and fiber tracts during normal aging remain poorly characterized, and it is unclear whether rates and patterns of brain aging differ by sex. This study used restriction spectrum imaging (RSI) to examine associations between age and brain microstructure in 147 community-dwelling participants (aged 56–99). Widespread associations with older age in multiple diffusion compartments, including increased free water, decreased restricted and hindered diffusion, and reduced neurite complexity, were observed diffusely in cortical gray matter, multiple white matter tracts, and the hippocampus. Age differences in cortical microstructure were largely independent of cortical thinning. Age-microstructure associations were mostly global, though regional foci of stronger effects emerged in fornix, anterior thalamic radiation and commissural fibers, as well as in medial temporal, orbitofrontal, and occipital cortex.

Address correspondence to Dr. Emilie T. Reas, Department of Neurosciences, Mail code 0841, UCSD, 9500 Gilman Dr., La Jolla, CA 92093-0841; ereas@ucsd.edu.

CREDIT AUTHOR STATEMENT:
Emilie T. Reas: Conceptualization, Formal analysis, Writing – Original draft
Donald J. Hagler, Jr.: Methodology, Software, Writing – Review & Editing
Murray J. Andrews: Methodology, Writing – Review & Editing
Roland R. Lee: Writing – Review & Editing
Anders M. Dale: Methodology, Software, Writing – Review & Editing
Linda K. McEvoy: Conceptualization, Supervision, Project Administration, Writing – Review & Editing, Funding acquisition

Author contributions

ETR and LKM conceived the study; ETR analyzed the data and wrote the manuscript; LKM oversaw data collection, advised on data analyses, and edited the manuscript. DJH advised on image analysis and edited the manuscript; MJA assisted with data processing and edited the manuscript. RRL reviewed the imaging data and edited the manuscript. AMD edited the manuscript.

Competing interests

A.M.D. is a Founder of and holds equity in CorTechs Labs, Inc, and serves on its Scientific Advisory Board. He is a member of the Scientific Advisory Board of Human Longevity, Inc. and receives funding through research agreements with General Electric Healthcare and Medtronic, Inc. The terms of these arrangements have been reviewed and approved by UCSD in accordance with its conflict of interest policies. L.K.M. holds equity in CorTechs Labs, Inc. The remaining authors declare that they have no conflict of interest.

Age differences in gray and white matter microstructure were stronger and more widespread for women than men, even after adjustment for education, hypertension and BMI. RSI may be a convenient, non-invasive tool for monitoring changes in gray and white matter diffusion properties thought to reflect reduced cellular fractions, neurite density, or neurite complexity, that occur with typical aging, and for detecting sex differences in patterns of brain aging.

Keywords

diffusion MRI; gray matter; microstructure; normal aging; white matter

1. Introduction

Structural remodeling of the human brain is a dynamic process that continues throughout the life-course from development to senescence. After brain maturation peaks in midlife, white matter compromise and gray matter atrophy appear, thought to underlie cognitive decline that typically emerges in later years. Although *in vivo* neuroimaging techniques carry the advantage over post-mortem histology of offering a window onto the healthy living brain, conventional MRI methods have been limited in their capacity to resolve the nuanced microstructure requisite to accurately characterize trajectories of neurobiological aging. Leveraging increasingly powerful tools to quantify the microstructural footprint of typical brain aging will be instrumental in identifying avenues for healthy neurobiological aging, and in developing approaches to preserve cognitive health and quality of life into later years.

Morphometric neuroimaging studies have reported widespread cortical thinning and volume loss in normal aging, with more severe atrophy accompanying neurodegenerative diseases. Whereas neuronal death contributes to atrophy in neurodegenerative disease, histological studies have demonstrated relative sparing of cell count in normal aging. Rather, cytoarchitectural changes in non-pathological aging include reduced axon and dendrite number, spine and synapse loss, and altered myelin morphology (Pannese, 2011). Thus, to better characterize normal brain aging, there is outstanding need to bridge this gap between post-mortem microscale and *in vivo* macroscale evidence with imaging techniques sensitive to morphometric alterations to neurites, synapses or cell bodies. Diffusion tensor imaging (DTI) studies, equipped to assess microstructure in living tissue, have consistently reported lower white matter fractional anisotropy (FA), a measure of the directional coherence of water diffusion, and higher mean diffusivity (MD), with older age (Bender et al., 2016; Bennett and Madden, 2014; Cox et al., 2016; de Groot et al., 2015). However, DTI measures an aggregate estimate of diffusion magnitude and direction within each voxel, obscuring contributions from cellular compartments that undergo non-uniform changes with aging or pathology, thus confounding estimates of tissue integrity (Chad et al., 2018).

Advances in imaging acquisition and modeling have overcome some of the limitations of DTI to more accurately characterize tissue microstructure. However, their applications to normal brain aging have been limited and inconclusive. Studies using advanced diffusion MRI methods such as neurite orientation dispersion and density imaging (NODDI) or diffusion kurtosis imaging (DKI) have reported reduced white matter neurite density, axonal

water fraction, and orientation dispersion with age (Benitez et al., 2018; Cox et al., 2016; Gong et al., 2014; Merluzzi et al., 2016). However, cortical gray matter microstructural changes have been minimally examined, with reports of increased free water, but no change in neurite density, and decreased, increased, or no change in orientation dispersion, with age (Merluzzi et al., 2016; Nazeri et al., 2015). These findings appear at odds with observed changes to dendrite morphology and complexity in the aged postmortem brain. Notably, these studies examined earlier life periods without focus on the oldest old (85+ years), with lower age bounds extending to middle age or young adulthood (Cox et al., 2016; Merluzzi et al., 2016; Nazeri et al., 2015). Advanced diffusion MRI investigations targeting older populations may improve sensitivity to subtle cytoarchitectural changes occurring in the final decades of life.

There is mounting evidence that men and women differ in susceptibility to risk factors for cognitive decline, biomarkers of Alzheimer's disease pathology, and disease progression, as well as in rates of cortical atrophy and lesion accumulation (Ferretti et al., 2018; Holland et al., 2013; Vinke et al., 2018). However, studies have observed weak and inconsistent sex differences in patterns of microstructural brain aging (Cox et al., 2016; Sullivan et al., 2001; Vinke et al., 2018). Further investigation is warranted to determine if sex differentially influences factors that promote brain aging.

Restriction spectrum imaging (RSI) uses multi-direction, multi-shell diffusion MRI to model diffusion orientation along a spectrum of apparent diffusion coefficients, from restricted to hindered to free diffusion. As demonstrated by White and colleagues in a histological validation study using rat brain tissue (White et al., 2013a), the scale of restricted diffusion is consistent with the size of neurites and small constrained spaces. Thus, restricted oriented (RO) diffusion likely reflects cylindrical compartments such as axons and dendrites, restricted isotropic diffusion (RI) may reflect small spherical spaces such as cell bodies or synapses, and crossing fibers (CF) reflect multi-directional restricted diffusion such as that in crossing or bending axons or complex dendritic architecture. Hindered isotropic (HI) and isotropic free water (IF) diffusion are consistent with extraneurite fractions such as large cell bodies or extracellular space, and CSF, respectively. RSI parameters may therefore be sensitive to changes in neurite density or complexity, axonal myelination, cell shrinkage or loss, or inflammation. RSI has been shown to be superior to DTI at fiber tractography in the presence of edema (McDonald et al., 2013), tumor delineation (White et al., 2013b), and assessing white matter pathology and treatment outcomes in temporal lobe epilepsy (Loi et al., 2016; McDonald et al., 2016). We previously found that restricted diffusion declines and IF increases with cognitive decline and amyloid pathology in prodromal Alzheimer's disease (Reas et al., in press; Reas et al., 2018; Reas et al., 2017). Though no studies have used RSI to examine normal brain aging, RSI may be a powerful tool for assessing changes to neurite or cell body architecture along the age spectrum.

We used RSI to examine associations of age with brain microstructure in community-dwelling older adults. Effects of age were evaluated on a range of microstructural properties across cortical gray matter and multiple white matter fibers to capture a comprehensive picture of microstructural brain aging. Regional microstructural changes were examined relative to whole-brain magnitudes to isolate areas most vulnerable to age-related injury, and

relative to cortical thinning to assess the independence of microstructural change from gray matter atrophy. Finally, we examined whether associations between age and RSI measures differed in strength or topography between men and women.

2. Material and Methods

2.1 Participants

Participants were members of the Rancho Bernardo Study (RBS) of Healthy Aging (Barrett-Connor, 2013), a longitudinal study of community-dwelling older adults in southern California, who completed a research visit in 2014–2016. Exclusion criteria included safety contraindication for MRI, history of stroke, neurological disease, head injury, or treatment for an alcohol use disorder. Of the 154 individuals who completed MRI, six were excluded due to poor data quality and one due to severe white matter disease, leaving data from 90 women and 57 men for analysis.

Study procedures were approved by the University of California, San Diego Human Research Protections Program Board and participants provided informed written consent prior to participation.

2.2 Health and lifestyle assessment

Education level was acquired at enrollment and converted to years of education. Height and weight were measured with the participant wearing light clothing and without shoes; body mass index (BMI, kg/m^2) was used as an estimate of obesity. Blood pressure was measured in seated, resting participants by a trained nurse and the mean of two readings, taken five minutes apart, was used for analysis. Participants were considered hypertensive if they had an average systolic blood pressure reading >140, diastolic blood pressure reading >90, were taking antihypertensive medication, or reported a physician diagnosis of hypertension. Information on smoking (never versus former; there were no current smokers), exercise (three or more times per week, yes/no), alcohol consumption (non-drinker/drinker), and history of diabetes was obtained from standard questionnaires.

2.3 Imaging data acquisition

MRI data were acquired on a 3.0 Tesla Discovery 750 scanner (GE Healthcare, Milwaukee, WI, USA) with an eight-channel phased array head coil at the UC San Diego Center for Functional MRI. The MRI sequences included a three-plane localizer; a sagittal 3D fast spoiled gradient echo T1-weighted volume optimized for maximum gray/white matter contrast (TE=3.2 ms, TR=8.1 ms, inversion time=600 ms, flip angle=8°, FOV=256×256 mm, matrix=256×192, slice thickness=1.2 mm, resampled to a resolution of 1×1×1.2 mm, scan time 8:27); an axial 2D single-shot pulsed-field gradient spin-echo echo-planar imaging sequence for measurement of RSI metrics (45-directions, one b=0 volume, plus b=500, 1500, 4000 s/mm^2 with 15 gradient directions for each non-zero b-value, TE=80.6 ms, TR=7 s, FOV=240×240 mm, matrix=96×96, slice thickness=2.5 mm, resampled to a resolution of 1.875×1.875×2.5 mm, scan time 6:34); and an axial 2D single-shot pulsed-field gradient spin-echo echo-planar imaging sequence for measurement of DTI metrics (one b=0 volume plus 30 gradient directions with b=1000 s/mm^2, TE=77.5 ms, TR=12 s, FOV=240×240 mm,

matrix=96×96, slice thickness=2.5 mm, resampled to a resolution of 1.875×1.875×2.5 mm, scan time 6:12. Both diffusion scans included an additional b=0 volume with reverse phase-encode polarity for B0 distortion correction.

2.4 Data processing

The automated processing stream was based on FreeSurfer (http://surfer.nmr.mgh.harvard.edu) with additional tools developed in-house, as previously described (Hagler Jr et al., 2019). RSI data were corrected for motion and eddy current (Zhuang et al., 2006), B_0 susceptibility (Holland et al., 2010), and gradient nonlinearity (Jovicich et al., 2006) distortions. Images were inspected and data containing uncorrectable artifacts were excluded. Using FreeSurfer's automated cortical reconstruction, gray matter, white matter, and CSF boundaries were delineated on the high-resolution T_1-weighted structural images and cortical thickness was computed as the distance between the white matter and pial surfaces (Fischl and Dale, 2000). RSI data were registered to the T_1 volume using mutual information (Wells et al., 1996) after coarse pre-alignment to atlas brains. Images were resampled to the original RSI acquisition resolution and the diffusion matrix was adjusted for head rotation. Resampling was performed using cubic interpolation and a registration matrix was created to specify the rigid-body transformation between RSI and T_1-weighted images. RSI metrics were computed and projected onto the cortical surface. To minimize partial volume effects from neighboring CSF and white matter, data were sampled within gray matter from up to 0.8–2.0 mm along the normal from the gray/white matter boundary, excluding data-points extending beyond the pial surface (Elman et al., 2017). To identify white matter fiber tracts, T_1 volumes were registered to a probabilistic atlas (AtlasTrack) (Hagler et al., 2009). Individual fiber path streamlines were then traced and labeled by comparing DTI-derived diffusion orientations to atlas fiber orientations. RI and HI were computed as the 0^{th} spherical harmonic coefficients of the restricted and hindered compartments, RO and CF were computed as the norm (square root of sum of squares) of the 2^{nd} and 4^{th} spherical harmonic coefficients of the restricted compartment, and IF was computed as the free water fraction. RSI measures were scaled by the norm of all fit coefficients. RSI and cortical thickness maps were registered to common space (*fsaverage)* and smoothed with a full-width half-max 10 mm kernel. Because fiber architecture is poorly characterized by the hindered fraction (White et al., 2013a), HI was not examined in white matter tracts. All other RSI metrics were computed in fifteen white matter fiber tracts. To minimize partial volume effects, voxels containing primarily gray matter or CSF were excluded from white matter tracts (Fischl et al., 2002). All RSI measures were computed in the hippocampus, automatically segmented according to a subcortical atlas (Fischl et al., 2002), due to its documented aging-related structural changes. FA and MD were computed from the DTI acquisition using standard, linear estimation with log-transformed diffusion-weighted signals.

2.5 Statistical analysis

Sex differences were assessed using independent sample t-tests for continuous variables, and chi-squared tests for categorical variables.

To examine associations between age and cortical microstructure, general linear models (GLM; *mri_glmfit*, without pruning) were run on gray matter RSI surface maps (RI, HI, RO, CF, IF) with a regressor of age. For comparison of age-related changes in cortical microstructure and thickness, GLMs were repeated on cortical thickness maps. To determine whether age-related changes in microstructure were independent of atrophy, RSI GLMs were conducted with age as a global regressor of interest, and cortical thickness as a vertex-wise covariate (--*prv* option in *mri_glmfit*). Pearson's correlations were computed between age and RSI measures in fiber tracts and hippocampus.

To identify regions in which age-microstructure associations were stronger or weaker than whole-brain associations, GLMs on RSI metrics were conducted with age as a regressor of interest and the respective global (mean across all cortical gray matter) RSI measure as a covariate. Partial correlations were calculated between age and fiber tract RSI metrics, adjusted for the global (mean across all fibers) RSI measure, and between age and hippocampal RSI metrics, adjusted for the global gray matter RSI measure.

To examine sex differences in age-microstructure associations, GLMs on cortical RSI surface maps and Pearson's correlations of age with fiber tract and hippocampal RSI measures were performed separately for men and women. Because of the larger sample of women, we conducted a sensitivity analysis to determine if sex differences were driven by group differences in statistical power. GLMs and correlations were repeated for a subgroup of 57 women matched in age to the group of 57 men. To examine whether sex differences in age-microstructure associations were mediated by differences in health risk factors, sex-stratified GLMs and correlations were repeated with adjustment for health or lifestyle variables that significantly differed ($p<0.05$) between men and women.

For comparison with DTI, correlations with age were repeated for fiber tract FA and for MD in the hippocampus, cortex, and white matter fibers.

Significance for cortical surface GLMs was set to $p<0.01$ and corrected for multiple comparisons using the false discovery rate (FDR). To further evaluate the topographic distribution of correlation effect sizes(Jernigan et al., 2003), Pearson's correlations were overlaid on the cortical surface. Significance for fiber tract and hippocampal ROI analyses was set to $p<0.003$ ($p<0.05$, Bonferroni adjusted for multiple comparisons across 16 regions).

Analyses were performed with Freesurfer version 5.3.0 and SPSS version 26.0 (IBM Corp, Armonk, NY, USA).

3. Results

3.1 Participant characteristics

Participant characteristics and global RSI measures by sex are shown in Table 1. Participants were 61% women and had a mean age of 76.6±7.8 years (range 56–99), with 33% over the age of 80 (Supplementary Figure 1). Women had a lower education level ($p<0.001$), BMI

(p=0.003), rates of hypertension (p=0.04), and mean cortical IF (p=0.005), and higher mean cortical HI (p=0.003), than men.

3.2 Associations between age and gray matter microstructure

Associations between age and cortical gray matter microstructure are presented in Figure 1 (p<0.01, FDR-corrected for multiple comparisons) and in Supplementary Figure 2 (un-thresholded Pearson's correlations). Older age was associated with lower RI and HI, and higher IF diffusely throughout most of bilateral cortex, largely sparing sensorimotor and inferior temporal regions. Age demonstrated both positive and negative correlations with RO and CF, and theses associations were more spatially restricted; RO and CF negatively correlated with age in occipital, orbitofrontal, and medial temporal cortex, and positively correlated with age in anterior cingulate and insula.

Correlations of age with fiber tract and hippocampal RSI metrics and are presented in Table 2. Age negatively correlated with hippocampal RI, RO, CF, and HI and positively correlated with hippocampal IF (p<0.001). Age negatively correlated with RI in all fiber tracts (p<0.001), with RO in all fiber tracts except cingulum, parahippocampal cingulum, SCS and SLF (p<0.003), and with CF in all fiber tracts except cingulum, CST, SIF and SCS (p<0.003). Age positively correlated with IF in all fiber tracts except parahippocampal cingulum (p<0.001).

3.3 Associations between age and microstructure, independent of atrophy

As shown in Figure 1, age was associated with widespread cortical thinning. Cortical thickness demonstrated considerable topographic overlap with isotropic diffusion but more weakly corelated with age than did microstructure. To determine if microstructural changes were accounted for by cortical atrophy, regressions between age and RSI measures were repeated with adjustment for vertex-wise cortical thickness (Figure 2). Comparison of Figures 1 and Figure 2 illustrates minimal change after controlling for atrophy, indicating that associations of age with all RSI metrics were largely independent of cortical thinning.

3.4 Associations between age and regional microstructure, beyond global microstructure

Associations of age with cortical microstructure, adjusted for the respective global RSI metric, are shown in Figure 3. Occipital, entorhinal, parahippocampal and orbitofrontal cortex demonstrated age-related reductions in restricted diffusion (RI, RO, CF) that significantly exceeded age-related changes across the whole brain. Higher anterior cingulate and insula RO and CF more strongly correlated with older age than observed globally.

Table 2 presents correlations of age with hippocampal and fiber tract microstructure, after adjustment for the respective global RSI metric. Age remained correlated with hippocampal RO, CF, and IF, anterior thalamic RO and CF, corpus callosum RO, forceps minor RO and CF, fornix RI, RO, CF, and IF, and striatal inferior frontal RI, indicating stronger than average age-related effects in these regions. Weaker than average age-related associations were observed for cingulum RO and CF, inferior frontal-superior frontal IF, superior corticostriatal CF and superior longitudinal fasciculus RO.

3.5 Sex differences in associations between age and microstructure

Older age correlated with lower global cortical RI and HI, and higher global IF for women and men, and with lower global CF for women (Supplementary Figure 3). Figure 4 (FDR-corrected) and Supplementary Figure 4 (un-thresholded) show regressions of age with cortical microstructure, stratified by sex. Older age in women was associated with widespread reductions in RI and HI, and increases in IF, with a comparable topography to that observed in the full sample. In men, age effects for HI and IF were weaker and more limited in distribution, and no associations with RI reached significance. Associations of age with RO and CF were comparable for men and women, though only those for women attained significance.

Age correlated with lower global fiber RI and RO, and higher global IF for women and men, and with lower global CF for women (Supplementary Figure 3). Consistent with the cortical surface results, age correlated with all RSI metrics across fiber tracts and hippocampus, more strongly for women than for men (Table 3).

To examine whether sex differences were attributable to power differences due to the larger sample of women, sex-stratified analyses were repeated on a subset of 57 women (77.3±7.9 (58–99) years) matched in age to the group of 57 men (77.3±7.9 (56–97) years). As shown in Supplementary Figure 5 and Supplementary Table 1, the age-RSI associations were only slightly attenuated in the subset of age-matched women, and the pattern of stronger effects for women remained.

Sex-stratified associations between age and RSI measures, adjusted for education, hypertension, and BMI, are shown in Supplementary Figure 6 and Supplementary Table 2. Associations between age and microstructure were slightly attenuated for both sexes, eliminating most correlations between age and gray matter microstructure in men. However, the robust sex differences in correlation strength remained after covariate adjustment.

3.6 Comparison with FA and MD

Older age was associated with higher MD throughout most of the cortex (Supplementary Figure 7), with a comparable topography to that for IF. Correlations between age and MD in hippocampus and fibers (Supplementary Table 3) were similar to those for IF (Table 2). Correlations between age and FA were comparable to those for RO, but were somewhat weaker than correlations for RI.

4. Discussion

This study used RSI to examine differences in brain microstructural properties with age in community-dwelling older adults. Results showed widespread increases in free water, accompanied by decreases in intraneurite and extraneurite diffusion and neurite complexity, in gray matter and white matter fibers with advancing age. Age-related microstructural differences varied topographically in strength and were largely independent of cortical atrophy. These findings expand upon prior reports that age-related microstructural injury is more prevalent in white matter than gray matter, to suggest that gray matter is similarly susceptible to cellular aging. Associations of age with microstructure were markedly

stronger for women than men, helping to clarify prior uncertainty over sex differences in brain aging and highlighting a heightened vulnerability to cytoarchitectural damage for aging women.

Consistent with prior evidence that white matter free water increases, and fractional anisotropy, neurite density, and fiber complexity decline with age (Benitez et al., 2018; Cox et al., 2016; Merluzzi et al., 2016), we observed increased free water and reduced restricted diffusion and fiber complexity with age in most fiber tracts examined. This may reflect age-related decline in axonal density or demyelination that has been documented in histological studies (Pannese, 2011). Though microstructural changes were notably widespread, the strongest effects were observed in fornix, anterior thalamic radiation and commissural fibers. While few studies have examined regional variations in the strength of white matter changes with age, relative to more widespread effects, Cox and colleagues (Cox et al., 2016) similarly reported particular susceptibility of thalamic radiations to older age.

Age was also associated with multiple gray matter RSI measures, building upon prior findings of increased gray matter free water with minimal effects on cortical neurite density or complexity (Merluzzi et al., 2016; Nazeri et al., 2015). Widespread free water increases, consistent with reports of increased cortical MD with age (Ni et al., 2010; Salminen et al., 2016) indicating expansion of the CSF space, topographically complemented reductions in restricted and hindered isotropic diffusion. Thus, the CSF space may expand in parallel with loss, shrinkage or dystrophy of neuronal or glial cell bodies, neurites, or synaptic compartments. Cortical RO and CF were also reduced, pointing to declining neurite density. Though dendrites may predominate in gray matter, prior studies demonstrating strong correspondence between cortical neurite density and myelin maps (Fukutomi et al., 2018) indicate that the RO and CF changes observed here may also signal reduced axon density within gray matter with age. These findings diverge from diffusion imaging studies in which gray matter neurite density and complexity were not reliably associated with age (Merluzzi et al., 2016; Nazeri et al., 2015), but align with histological evidence for age-related loss of dendrites, spines and synapses (Pannese, 2011). The subtle cytoarchitectural changes detectable here may be attributable to the more nuanced characterization of tissue architecture by RSI compared to other diffusion models, such as the inclusion of restricted isotropic and hindered volume fractions, or to the older age range and relative homogeneity of the RBS population. Notably, age-related microstructural changes remained after accounting for cortical thickness, suggesting that RSI characterizes cortical structure based upon information that is independent of atrophy. However, these findings should be interpreted with caution, as correction for cortical thickness may not fully capture contributions from atrophy if diffusion parameters and thickness are not linearly related (Metzler-Baddeley et al., 2012).

Correlations with age were generally comparable between FA and RO, and between MD and IF. These findings highlight the consistency of RSI with expected age-related free water increases and reductions in white matter oriented diffusion that have been widely reported in prior studies (Bender et al., 2016; Bennett and Madden, 2014; Cox et al., 2016; de Groot et al., 2015; Ni et al., 2010; Salminen et al., 2016). However, additional age differences were observed for restricted (RI, CF) and hindered (HI) diffusion, including stronger age

correlations for RI than FA, pointing to further cytoarchitectural changes with age beyond those captured by conventional DTI.

We observed the strongest age-dependent microstructural compromise localized to occipital, orbitofrontal and medial temporal cortex. Although the retrogenesis hypothesis of aging posits that later developing white matter tracts and cortical regions, including frontal and parietal cortex, are earliest to degenerate (Raz, 2000), we were unable to assess the earliest age-related changes, given the age range of our sample. Age-related frontal and medial temporal atrophy, in line with our results, have been commonly found (Fjell et al., 2009a; Thambisetty et al., 2010), whereas occipital thinning has been less often reported. Other studies including participants over age 90 have also observed occipital atrophy (Fjell et al., 2009a; Salat et al., 2004), which is magnified in older age relative to midlife (McGinnis et al., 2011). Thus, the posterior cortical thinning found in our sample, which included a large number of the oldest old and few in middle age (33% between ages 80–99, 2% under age 60), may be characteristic of atrophy patterns in the latest decades of life.

Unexpectedly, RO, CF, and cortical thickness increased with age in anterior cingulate and insula. Though the basis of this finding cannot be resolved from this study, one possibility is particular resilience of these areas to brain aging, supported by prior reports that anterior cingulate thickness is relatively spared with age (Fjell et al., 2009b). These regions exhibit a distinct preponderance of von Economo neurons, which show marked stability of number in older age (Allman et al., 2011) and are abundant in “SuperAgers” aged 80 years or more with exceptional memory (Gefen et al., 2015). Here, if selection bias favors preserved brain health with age, estimates of microstructural integrity may be inflated in the oldest of our sample. Consistent with this explanation, Fjell and colleagues (Fjell et al., 2006) observed that, compared to both young adults and average-performing older adults, older adults with high fluid abilities had greater thickness with age in posterior cingulate and subcallosal gyrus, regions neighboring those showing age-related increases in RO/CF here. Longitudinal investigation is needed to evaluate within-subject increases in RO or CF over time, which may reflect compensatory dendritic sprouting or increased axonal density.

Associations between age and microstructure were stronger for women than men, even after considering sample size imbalances, and after adjusting for differences in education, BMI, and hypertension. These striking sex differences help to resolve previous ambiguity regarding sex differences in microstructural changes with age (Cox et al., 2016; Sullivan et al., 2001; Vinke et al., 2018). Further, they corroborate evidence that risk for cognitive decline and rates of atrophy preceding dementia are greater for women, and that risk factors for cognitive impairment, and the expression of brain pathology differ between men and women (Ferretti et al., 2018). During midlife, decline in diffusion MRI parameters of brain microstructure has been found to begin earlier in men (age 29) than women (age 43) (Toschi et al., 2019), raising the possibility that for women, cytoarchitectural brain changes are delayed and may be more pronounced in later decades. Typical neurobiological aging may be accelerated in women due to differences in genetics, hormones, or life-course exposure to lifestyle risk factors, which may enhance vulnerability to disease and exacerbate clinical and cognitive manifestations (Andrew and Tierney, 2018). Survivor bias may also contribute to

the observed sex differences. Further research will aid in elucidating health, sociocultural, or hormonal factors that may hasten brain aging for women.

The RBS population compromises mostly white, educated, relatively healthy middle-class Americans, which limits generalizability of our observed patterns of brain aging to more diverse or less healthy cohorts. However, these properties also minimize confounding due to variance in socioeconomic status or access to healthcare. Considering the age range of our sample, we cannot exclude the possibility that latent Alzheimer's disease pathology contributed to our brain measures. Because cross-sectional studies are susceptible to survivor bias and may over- or underestimate effects of chronological aging (Nyberg et al., 2010; Raz et al., 2005), longitudinal investigations are needed to help clarify how age drives intra-individual microstructural changes. The RSI acquisition is not necessarily optimized and may be further improved with different b-values or a greater number of diffusion directions, though with a tradeoff of longer acquisition time. Finally, because RSI is a biophysical model of diffusion patterns that indirectly approximates underlying cellular architecture, caution should be taken in inferring the neurobiological origin of the age-related differences in diffusion properties reported here.

5. Conclusions

This study identified associations of age with widespread gray and white matter microstructural compromise that were more pronounced for women than for men. Aging may induce significant changes to neuronal or glial architecture even in the absence of gross cell loss and atrophy. RSI may be a convenient, non-invasive tool for monitoring neurobiological aging and for assessing efficacy of lifestyle interventions intended to preserve brain health in later life.

Supplementary Material

Refer to Web version on PubMed Central for supplementary material.

Funding

This work was supported by the National Institute on Alcohol Abuse and Alcoholism (R01 AA021187), National Institute on Aging (R01 AG062483, K99 AG057797), National Institute on Drug Abuse (grant number 1U24DA041123-01), a training fellowship to ETR under National Institutes of Health (1P30AG062429), and a Warren Alpert Distinguished Scholars Award to ETR (20192684).

References

Allman JM, Tetreault NA, Hakeem AY, Manaye KF, Semendeferi K, Erwin JM, Park S, Goubert V, Hof PR, 2011 The von Economo neurons in the frontoinsular and anterior cingulate cortex. Ann N Y Acad Sci 1225, 59–71. [PubMed: 21534993]

Andrew MK, Tierney MC, 2018 The puzzle of sex, gender and Alzheimer's disease: Why are women more often affected than men? Women's Health 14, 1745506518817995.

Barrett-Connor E, 2013 The Rancho Bernardo Study: 40 years studying why women have less heart disease than men and how diabetes modifies women's usual cardiac protection. Glob Heart 8(2).

Bender AR, Volkle MC, Raz N, 2016 Differential aging of cerebral white matter in middle-aged and older adults: A seven-year follow-up. Neuroimage 125, 74–83. [PubMed: 26481675]

Benitez A, Jensen JH, Falangola MF, Nietert PJ, Helpern JA, 2018 Modeling white matter tract integrity in aging with diffusional kurtosis imaging. Neurobiol Aging 70, 265–275. [PubMed: 30055412]

Bennett IJ, Madden DJ, 2014 Disconnected aging: cerebral white matter integrity and age-related differences in cognition. Neuroscience 276, 187–205. [PubMed: 24280637]

Chad JA, Pasternak O, Salat DH, Chen JJ, 2018 Re-examining age-related differences in white matter microstructure with free-water corrected diffusion tensor imaging. Neurobiol Aging 71, 161–170. [PubMed: 30145396]

Cox SR, Ritchie SJ, Tucker-Drob EM, Liewald DC, Hagenaars SP, Davies G, Wardlaw JM, Gale CR, Bastin ME, Deary IJ, 2016 Ageing and brain white matter structure in 3,513 UK Biobank participants. Nat Commun 7, 13629. [PubMed: 27976682]

de Groot M, Ikram MA, Akoudad S, Krestin GP, Hofman A, van der Lugt A, Niessen WJ, Vernooij MW, 2015 Tract-specific white matter degeneration in aging: the Rotterdam Study. Alzheimers Dement 11(3), 321–330. [PubMed: 25217294]

Elman JA, Panizzon MS, Hagler DJ Jr., Fennema-Notestine C, Eyler LT, Gillespie NA, Neale MC, Lyons MJ, Franz CE, McEvoy LK, Dale AM, Kremen WS, 2017 Genetic and environmental influences on cortical mean diffusivity. Neuroimage 146, 90–99. [PubMed: 27864081]

Ferretti MT, Iulita MF, Cavedo E, Chiesa PA, Schumacher Dimech A, Santuccione Chadha A, Baracchi F, Girouard H, Misoch S, Giacobini E, Depypere H, Hampel H, Women's Brain, P., the Alzheimer Precision Medicine, I., 2018 Sex differences in Alzheimer disease - the gateway to precision medicine. Nat Rev Neurol.

Fischl B, Dale AM, 2000 Measuring the thickness of the human cerebral cortex from magnetic resonance images. Proc Natl Acad Sci U S A 97(20), 11050–11055. [PubMed: 10984517]

Fischl B, Salat DH, Busa E, Albert M, Dieterich M, Haselgrove C, van der Kouwe A, Killiany R, Kennedy D, Klaveness S, Montillo A, Makris N, Rosen B, Dale AM, 2002 Whole brain segmentation: automated labeling of neuroanatomical structures in the human brain. Neuron 33(3), 341–355. [PubMed: 11832223]

Fjell AM, Walhovd KB, Fennema-Notestine C, McEvoy LK, Hagler DJ, Holland D, Brewer JB, Dale AM, 2009a One-year brain atrophy evident in healthy aging. J Neurosci 29(48), 15223–15231. [PubMed: 19955375]

Fjell AM, Walhovd KB, Reinvang I, Lundervold A, Salat D, Quinn BT, Fischl B, Dale AM, 2006 Selective increase of cortical thickness in high-performing elderly--structural indices of optimal cognitive aging. Neuroimage 29(3), 984–994. [PubMed: 16176876]

Fjell AM, Westlye LT, Amlien I, Espeseth T, Reinvang I, Raz N, Agartz I, Salat DH, Greve DN, Fischl B, Dale AM, Walhovd KB, 2009b High consistency of regional cortical thinning in aging across multiple samples. Cereb Cortex 19(9), 2001–2012. [PubMed: 19150922]

Fukutomi H, Glasser MF, Zhang H, Autio JA, Coalson TS, Okada T, Togashi K, Van Essen DC, Hayashi T, 2018 Neurite imaging reveals microstructural variations in human cerebral cortical gray matter. Neuroimage 182, 488–499. [PubMed: 29448073]

Gefen T, Peterson M, Papastefan ST, Martersteck A, Whitney K, Rademaker A, Bigio EH, Weintraub S, Rogalski E, Mesulam MM, Geula C, 2015 Morphometric and histologic substrates of cingulate integrity in elders with exceptional memory capacity. J Neurosci 35(4), 1781–1791. [PubMed: 25632151]

Gong N-J, Wong C-S, Chan C-C, Leung L-M, Chu Y-C, 2014 Aging in deep gray matter and white matter revealed by diffusional kurtosis imaging. Neurobiology of aging 35(10), 2203–2216. [PubMed: 24910392]

Hagler DJ Jr., Ahmadi ME, Kuperman J, Holland D, McDonald CR, Halgren E, Dale AM, 2009 Automated white-matter tractography using a probabilistic diffusion tensor atlas: Application to temporal lobe epilepsy. Hum Brain Mapp 30(5), 1535–1547. [PubMed: 18671230]

Hagler DJ Jr, Hatton S, Cornejo MD, Makowski C, Fair DA, Dick AS, Sutherland MT, Casey B, Barch DM, Harms MP, 2019 Image processing and analysis methods for the Adolescent Brain Cognitive Development Study. NeuroImage 202, 116091. [PubMed: 31415884]

Holland D, Desikan RS, Dale AM, McEvoy LK, 2013 Higher rates of decline for women and apolipoprotein E ε4 carriers. American Journal of Neuroradiology 34(12), 2287–2293. [PubMed: 23828104]

Holland D, Kuperman JM, Dale AM, 2010 Efficient correction of inhomogeneous static magnetic field-induced distortion in Echo Planar Imaging. Neuroimage 50(1), 175–183. [PubMed: 19944768]

Jernigan TL, Gamst AC, Fennema-Notestine C, Ostergaard AL, 2003 More "mapping" in brain mapping: statistical comparison of effects. Hum Brain Mapp 19(2), 90–95. [PubMed: 12768533]

Jovicich J, Czanner S, Greve D, Haley E, van der Kouwe A, Gollub R, Kennedy D, Schmitt F, Brown G, Macfall J, Fischl B, Dale A, 2006 Reliability in multi-site structural MRI studies: effects of gradient non-linearity correction on phantom and human data. Neuroimage 30(2), 436–443. [PubMed: 16300968]

Loi RQ, Leyden KM, Balachandra A, Uttarwar V, Hagler DJ Jr., Paul BM, Dale AM, White NS, McDonald CR, 2016 Restriction spectrum imaging reveals decreased neurite density in patients with temporal lobe epilepsy. Epilepsia.

McDonald CR, Delfanti RL, Krishnan AP, Leyden KM, Hattangadi-Gluth JA, Seibert TM, Karunamuni R, Elbe P, Kuperman JM, Bartsch H, Piccioni DE, White NS, Dale AM, Farid N, 2016 Restriction spectrum imaging predicts response to bevacizumab in patients with high-grade glioma. Neuro Oncol 18(11), 1579–1590. [PubMed: 27106406]

McDonald CR, White NS, Farid N, Lai G, Kuperman JM, Bartsch H, Hagler DJ, Kesari S, Carter BS, Chen CC, Dale AM, 2013 Recovery of white matter tracts in regions of peritumoral FLAIR hyperintensity with use of restriction spectrum imaging. AJNR Am J Neuroradiol 34(6), 1157–1163. [PubMed: 23275591]

McGinnis SM, Brickhouse M, Pascual B, Dickerson BC, 2011 Age-related changes in the thickness of cortical zones in humans. Brain topography 24(3–4), 279–291. [PubMed: 21842406]

Merluzzi AP, Dean DC 3rd, Adluru N, Suryawanshi GS, Okonkwo OC, Oh JM, Hermann BP, Sager MA, Asthana S, Zhang H, Johnson SC, Alexander AL, Bendlin BB, 2016 Age-dependent differences in brain tissue microstructure assessed with neurite orientation dispersion and density imaging. Neurobiol Aging 43, 79–88. [PubMed: 27255817]

Metzler-Baddeley C, O'Sullivan MJ, Bells S, Pasternak O, Jones DK, 2012 How and how not to correct for CSF-contamination in diffusion MRI. Neuroimage 59(2), 1394–1403. [PubMed: 21924365]

Nazeri A, Chakravarty MM, Rotenberg DJ, Rajji TK, Rathi Y, Michailovich OV, Voineskos AN, 2015 Functional consequences of neurite orientation dispersion and density in humans across the adult lifespan. J Neurosci 35(4), 1753–1762. [PubMed: 25632148]

Ni JM, Chen S, Liu JJ, Huang G, Shen TZ, Chen XR, 2010 Regional diffusion changes of cerebral grey matter during normal aging--a fluid-inversion prepared diffusion imaging study. Eur J Radiol 75(2), 134–138. [PubMed: 19443158]

Nyberg L, Salami A, Andersson M, Eriksson J, Kalpouzos G, Kauppi K, Lind J, Pudas S, Persson J, Nilsson LG, 2010 Longitudinal evidence for diminished frontal cortex function in aging. Proc Natl Acad Sci U S A 107(52), 22682–22686. [PubMed: 21156826]

Pannese E, 2011 Morphological changes in nerve cells during normal aging. Brain Struct Funct 216(2), 85–89. [PubMed: 21431333]

Raz N, 2000 Aging of the brain and its impact on cognitive performance: Integration of structural and functional findings.

Raz N, Lindenberger U, Rodrigue KM, Kennedy KM, Head D, Williamson A, Dahle C, Gerstorf D, Acker JD, 2005 Regional brain changes in aging healthy adults: general trends, individual differences and modifiers. Cereb Cortex 15(11), 1676–1689. [PubMed: 15703252]

Reas ET, Hagler DJ Jr., White NS, Kuperman JM, Bartsch H, Cross K, Loi RQ, Balachandra AR, Meloy MJ, Wierenga CE, Galasko D, Brewer JB, Dale AM, McEvoy LK, 2017 Sensitivity of restriction spectrum imaging to memory and neuropathology in Alzheimer's disease. Alzheimer's research & therapy 9(1), 55.

Reas ET, Hagler DJ, Kuperman J, Wierenga CE, Galasko D, White NS, Dale AM, Banks SJ, McEvoy LK, Brewer JB, in press Associations between microstructure, amyloid, and cognition in amnestic mild cognitive impairment and dementia. Journal of Alzheimer's Disease.

Reas ET, Hagler DJ, White NS, Kuperman J, Bartsch H, Wierenga CE, Galasko D, Brewer JB, Dale AM, McEvoy LK, 2018 Microstructural brain changes track cognitive decline in mild cognitive impairment. Neuroimage: Clinical.

Salat DH, Buckner RL, Snyder AZ, Greve DN, Desikan RS, Busa E, Morris JC, Dale AM, Fischl B, 2004 Thinning of the cerebral cortex in aging. Cereb Cortex 14(7), 721–730. [PubMed: 15054051]

Salminen LE, Conturo TE, Laidlaw DH, Cabeen RP, Akbudak E, Lane EM, Heaps JM, Bolzenius JD, Baker LM, Cooley S, Scott S, Cagle LM, Phillips S, Paul RH, 2016 Regional age differences in gray matter diffusivity among healthy older adults. Brain Imaging Behav 10(1), 203–211. [PubMed: 25864197]

Sullivan EV, Adalsteinsson E, Hedehus M, Ju C, Moseley M, Lim KO, Pfefferbaum A, 2001 Equivalent disruption of regional white matter microstructure in ageing healthy men and women. NeuroReport 12(1), 99–104. [PubMed: 11201100]

Thambisetty M, Wan J, Carass A, An Y, Prince JL, Resnick SM, 2010 Longitudinal changes in cortical thickness associated with normal aging. Neuroimage 52(4), 1215–1223. [PubMed: 20441796]

Toschi N, Gisbert RA, Passamonti L, Canals S, De Santis S, 2019 Multi-shell diffusion imaging reveals sex-specific trajectories of early white matter degeneration in normal aging. Neurobiology of Aging.

Vinke EJ, de Groot M, Venkatraghavan V, Klein S, Niessen WJ, Ikram MA, Vernooij MW, 2018 Trajectories of imaging markers in brain aging: the Rotterdam Study. Neurobiol Aging 71, 32–40. [PubMed: 30077040]

Wells WM 3rd, Viola P, Atsumi H, Nakajima S, Kikinis R, 1996 Multi-modal volume registration by maximization of mutual information. Med Image Anal 1(1), 35–51. [PubMed: 9873920]

White NS, Leergaard TB, D'Arceuil H, Bjaalie JG, Dale AM, 2013a Probing tissue microstructure with restriction spectrum imaging: Histological and theoretical validation. Hum Brain Mapp 34(2), 327–346. [PubMed: 23169482]

White NS, McDonald CR, Farid N, Kuperman JM, Kesari S, Dale AM, 2013b Improved conspicuity and delineation of high-grade primary and metastatic brain tumors using "restriction spectrum imaging": quantitative comparison with high B-value DWI and ADC. AJNR Am J Neuroradiol 34(5), 958–964, S951. [PubMed: 23139079]

Zhuang J, Hrabe J, Kangarlu A, Xu D, Bansal R, Branch CA, Peterson BS, 2006 Correction of eddy-current distortions in diffusion tensor images using the known directions and strengths of diffusion gradients. Journal of magnetic resonance imaging : JMRI 24(5), 1188–1193. [PubMed: 17024663]

HIGHLIGHTS:

- We used RSI to assess associations between age and brain microstructure
- Age correlated with restricted, hindered and free diffusion in cortex and fibers
- Age-RSI associations were stronger and more widespread for women than for men
- Gray matter age-RSI associations persisted after controlling for cortical thickness
- Regional age-RSI associations emerged after adjusting for whole-brain RSI

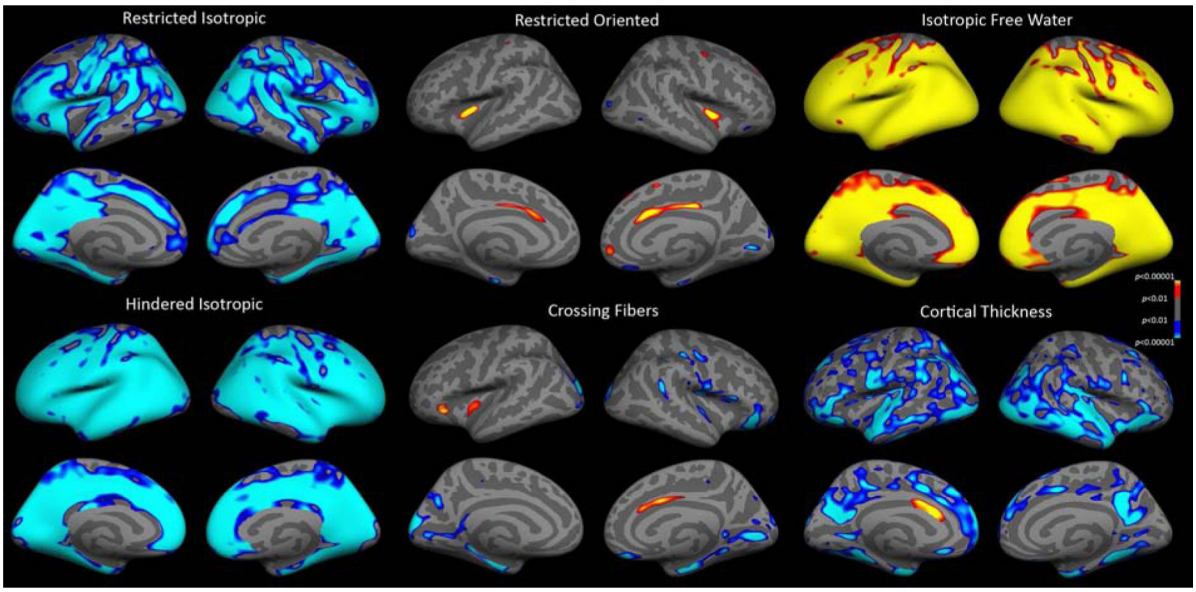

Figure 1. Associations of age with cortical microstructure and thickness.

Warm colors indicate positive correlations and cool colors indicate negative correlations, of age with gray matter RSI metrics (RI, HI, RO, CF, IF) and cortical thickness (p<0.01, FDR corrected).

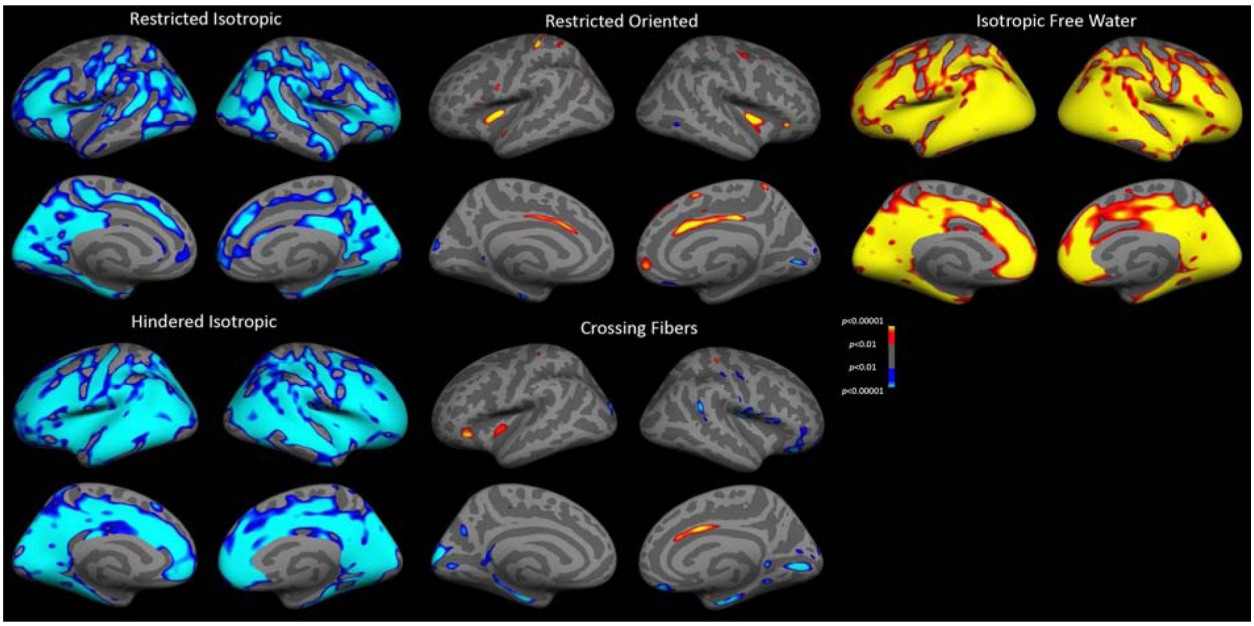

Figure 2. Associations between age and cortical microstructure, controlling for cortical thickness.

Figure conventions are the same as for Figure 1.

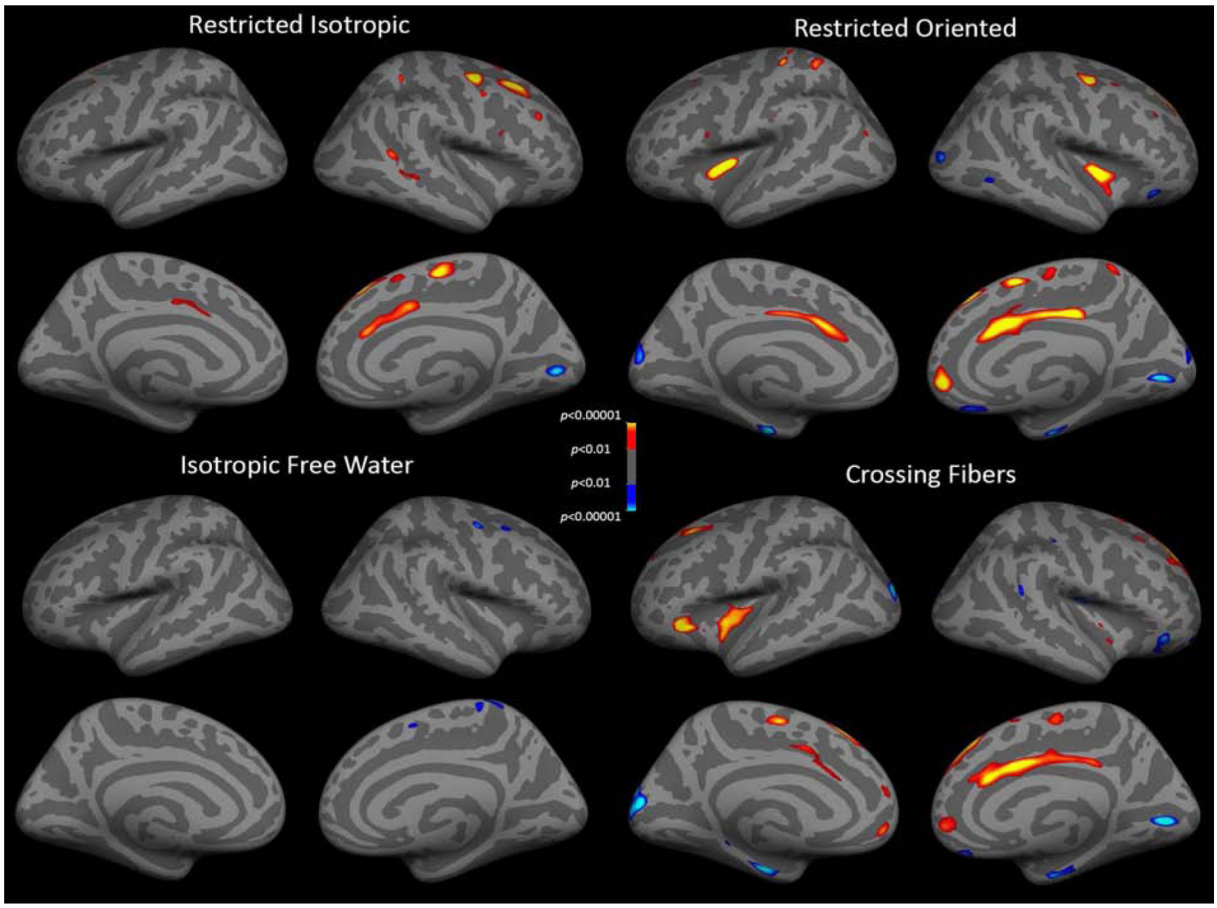

Figure 3. Associations between age and cortical microstructure, controlling for global microstructure.

RSI metrics are adjusted for the respective global (mean across all gray matter) RSI metric. Figure conventions are the same as for Figure 1.

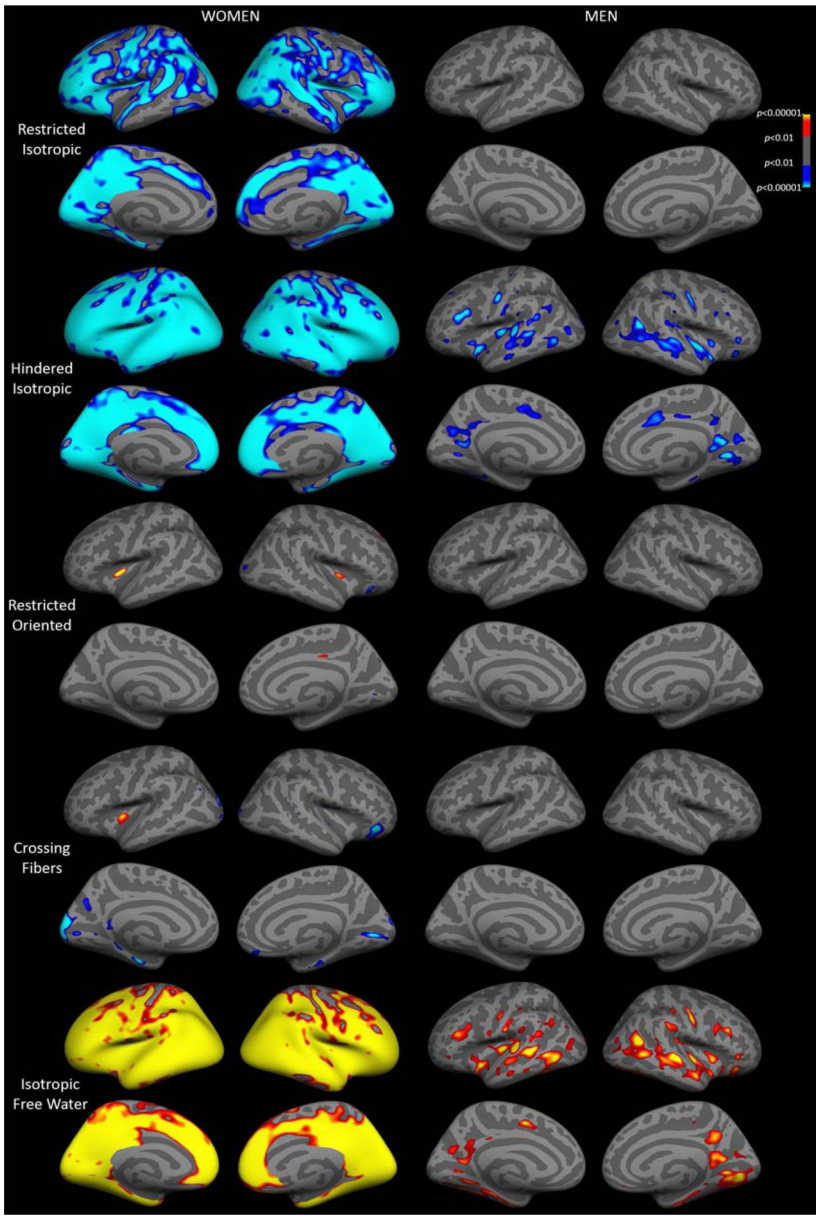

Figure 4. Associations between age and cortical microstructure, stratified by sex.
Figure conventions are the same as for Figure 1.

Table 1.

Participant characteristics and global RSI measures by sex (mean±SD unless otherwise noted).

	Women (*N*=90)	**Men (*N*=57)**
Age (years)	76.2±7.8	77.3±7.9
Education (years)	14.4±1.9	15.8±2.0 ***
Exercise (% 3+times/week)	74	79
Smoking (% ever)	37	47
Alcohol consumption (% drinker)	87	82
BMI	25.2±4.3	27.1±3.1 **
Hypertension (%)	53	70 *
Diabetes (%)	8	16
3MS (adjusted for age and education)	94.8±4.6	94.9±4.8
Fiber RI	0.42±0.03	0.42±0.02
Fiber RO	0.55±0.02	0.55±0.02
Fiber CF	0.22±0.01	0.23±0.01
Fiber IF	0.25±0.03	0.26±0.03
Gray matter RI	0.29±0.02	0.29±0.02
Gray matter RO	0.19±0.01	0.18±0.01
Gray matter CF	0.11±0.01	0.11±0.01
Gray matter HI	0.74±0.04	0.72±0.04 **
Gray matter IF	0.41±0.06	0.44±0.06 **

* $p<0.05$,

** $p<0.01$,

*** $p<0.001$

3MS=Modified Mini-Mental State Test; BMI=body mass index; CF=crossing fibers; HI=hindered isotropic; IF=isotropic free water; RI=restricted isotropic; RO=restricted oriented

Table 2.

Pearson's correlations (*r*) or partial correlations (*r*, adjusted for global RI, RO, CF, HI, or IF) between age and hippocampus or fiber tract RI, RO, CF, HI and IF.

	r					**Partial *r*(adjusted for global RSI)**				
	RI	**RO**	**CF**	**HI**	**IF**	**RI**	**RO**	**CF**	**HI**	**IF**
Hippocampus	**−0.37**	**−0.44**	**−0.39**	**−0.35**	**0.54**	−0.12	**−0.45**	**−0.30**	−0.03	**0.25**
ATR	**−0.62**	**−0.51**	**−0.51**	-	**0.64**	−0.23	**−0.27**	**−0.37**	-	0.20
Cingulum	**−0.53**	−0.05	0.12	-	**0.36**	−0.01	**0.31**	**0.30**	-	−0.11
Corpus callosum	**−0.63**	**−0.54**	**−0.42**	-	**0.62**	−0.16	**−0.26**	−0.20	-	0.09
CST	**−0.49**	**−0.32**	−0.14	-	**0.56**	0.03	−0.09	0.17	-	0.12
Forceps major	**−0.47**	**−0.38**	**−0.25**	-	**0.55**	0.01	−0.07	0.03	-	0.15
Forceps minor	**−0.58**	**−0.55**	**−0.46**	-	**0.49**	−0.14	**−0.30**	**−0.29**	-	−0.09
Fornix	**−0.63**	**−0.63**	**−0.59**	-	**0.66**	**−0.35**	**−0.48**	**−0.51**	-	**0.40**
IFO	**−0.54**	**−0.40**	**−0.30**	-	**0.61**	0.11	0.02	−0.02	-	0.10
IFSF	**−0.54**	**−0.31**	**−0.36**	-	**0.45**	0.06	0.11	−0.09	-	**−0.25**
ILF	**−0.46**	**−0.31**	**−0.31**	-	**0.46**	0.17	0.14	−0.05	-	−0.12
Parahippocampal cingulum	**−0.34**	−0.15	**−0.39**	-	0.20	0.02	0.06	−0.23	-	0.00
SCS	**−0.51**	−0.16	−0.07	-	**0.52**	0.16	0.11	**0.41**	-	−0.04
SIF	**−0.64**	**−0.26**	−0.20	-	**0.51**	**−0.25**	0.08	0.13	-	−0.09
SLF	**−0.47**	−0.14	**-0.29**	-	**0.44**	0.20	**0.34**	0.04	-	−0.19
Uncinate	**−0.57**	−0.33	**−0.28**	-	**0.49**	−0.10	0.05	−0.01	-	−0.09

Bold values are significant at $p<0.003$.

HI was not examined in fiber tracts due to its poor characterization of white matter microstructure.

ATR=anterior thalamic radiation, CF=crossing fibers, CST=corticospinal tract, HI=hindered isotropic, IF=isotropic free water, IFO=inferior frontal occipital, IFSF=inferior frontal superior frontal, ILF=inferior longitudinal fasciculus, RI=restricted isotropic, RO=restricted oriented, SCS=superior corticostriatal, SIF=striatal inferior frontal, SLF=superior longitudinal fasciculus

Table 3.

Pearson's correlations (*r*) between age and hippocampus and fiber tract RSI measures separately for men and women.

	Women					Men				
	RI	**RO**	**CF**	**HI**	**IF**	**RI**	**RO**	**CF**	**HI**	**IF**
Hippocampus	−0.37	**−0.49**	**−0.41**	−0.42	**0.62**	−0.38	−0.34	−0.36	−0.24	**0.40**
ATR	−0.69	−0.59	−0.58		**0.72**	**−0.48**	−0.37	**−0.40**		**0.50**
Cingulum	−0.61	−0.07	0.06		**0.31**	**−0.44**	−0.03	0.16		**0.44**
Corpus callosum	**−0.74**	−0.67	−0.53		**0.72**	−0.45	−0.33	−0.28		**0.46**
CST	−0.55	−0.37	−0.19		**0.61**	−0.37	−0.28	−0.10		**0.49**
Forceps major	−0.63	**−0.49**	**−0.31**		**0.66**	−0.27	−0.23	−0.19		**0.43**
Forceps minor	−0.65	−0.63	−0.52		**0.57**	**−0.46**	**−0.40**	−0.39		0.34
Fornix	−0.69	−0.68	−0.63		**0.73**	−0.56	−0.57	−0.55		**0.60**
IFO	−0.62	**−0.51**	−0.39		**0.71**	**−0.40**	−0.21	−0.15		**0.49**
IFSF	**−0.64**	−0.38	−0.52		**0.53**	−0.36	−0.18	−0.11		0.32
ILF	−0.49	**−0.40**	−0.33		**0.58**	**−0.41**	−0.16	−0.28		0.32
Parahippocampal cingulum	−0.37	−0.25	−0.38		0.20	−0.38	−0.01	**−0.41**		0.21
SCS	−0.71	−0.36	−0.35		**0.61**	−0.53	−0.10	−0.01		0.33
SIF	−0.59	−0.27	−0.21		**0.59**	−0.36	0.02	0.07		**0.41**
SLF	**−0.54**	−0.20	−0.40		**0.45**	−0.35	−0.09	−0.16		**0.44**
Uncinate	−0.63	**−0.45**	**−0.40**		**0.60**	−0.49	−0.11	−0.08		0.32

See footnotes for Table 2.